

## RESEARCH ARTICLE

10.1002/2016JA022398

## Key Points:

- A sign of coupling of tropical cyclone and irregularities/scintillation is first time observed from Hong Kong
- Both ground- and space-based GPS observations record ionospheric responses to the tropical cyclone
- It is suspected that gravity waves might be generated and seed Rayleigh-Taylor instability, leading to ionospheric irregularities

## Correspondence to:

Z. Liu,  
lszzliu@polyu.edu.hk

## Citation:

Yang, Z., and Z. Liu (2016), Observational study of ionospheric irregularities and GPS scintillations associated with the 2012 tropical cyclone Tembin passing Hong Kong, *J. Geophys. Res. Space Physics*, 121, 4705–4717, doi:10.1002/2016JA022398.

Received 16 JAN 2016

Accepted 11 APR 2016

Accepted article online 13 APR 2016

Published online 12 MAY 2016

## Observational study of ionospheric irregularities and GPS scintillations associated with the 2012 tropical cyclone Tembin passing Hong Kong

Zhe Yang<sup>1</sup> and Zhizhao Liu<sup>1</sup><sup>1</sup>Now at Department of Land Surveying and Geo-Informatics, Hong Kong Polytechnic University, Kowloon, Hong Kong

**Abstract** This study presents the ionospheric responses observed in Hong Kong to a Typhoon, namely, Tembin, from the aspects of the occurrence of ionospheric irregularities and scintillations, using Global Positioning System (GPS) observations from a ground-based GPS scintillation monitoring station in Hong Kong and from GPS receivers on board the Constellation Observing System for Meteorology, Ionosphere, and Climate (COSMIC) satellites. The ionospheric irregularities and scintillations are characterized by the rate of total electron content variation index (ROTI) and the amplitude scintillation index  $S_4$ , respectively. The typhoon Tembin formed over the western North Pacific during 18–30 August 2012 and approached Hong Kong during 24–27 August 2012 with the closest distance 290 km from Hong Kong at around 17 universal time (UT) on 25 August 2012. The ground-based observations indicate that in the nighttime period of 20:00–02:00 local time (LT = UT + 8 h) on 26 August when Tembin passed closely to Hong Kong, the ionospheric irregularities and scintillations of GPS signals were observed in the south of Hong Kong, over the area of 13°N ~ 23°N in latitude and 110°E ~ 120°E in longitude. From the COSMIC observations, it shows that the number of radio occultation scintillation events peaks on 26 August 2012 during the passage of Tembin. Without the presence of strong geomagnetic or solar activity, it is suspected that gravity waves might be generated in the lower atmosphere and likely seed the formation of ionospheric plasma irregularities. This work for the first time from Hong Kong observes the sign of coupling between the lower atmosphere and ionosphere in a tropical cyclone event, combining both ground- and space-based GPS observation data.

### 1. Introduction

Ionospheric scintillation as one of the earliest known effects of space weather [Hey *et al.*, 1946] is a major issue in the Global Positioning System (GPS)/Global Navigation Satellite System (GNSS), because it can result in cycle slips or even complete loss of lock of GNSS signals [Kintner *et al.*, 2007]. Affected by ionospheric scintillations, GNSS in return becomes a powerful tool to investigate scintillations and the formation and evolution of ionospheric irregularities that generate scintillations. In the past, a lot of research has studied the characteristics of ionospheric scintillations [e.g., Caton and Groves, 2006; Dymond, 2012; Jiao *et al.*, 2013], ionospheric irregularities that cause scintillations [e.g., Basu *et al.*, 1996; Dandekar and Groves, 2004; Muella *et al.*, 2008], and the effects of solar and magnetic activity on occurrences of irregularities and scintillations of radio signals [e.g., Bhattacharyya *et al.*, 2002; Shi *et al.*, 2011].

Meteorological processes in the lower atmosphere have demonstrated to cause ionospheric variability [Chernigovskaya *et al.*, 2015; Goncharenko and Zhang, 2008; Kazimirovsky, 2002; Korenkov *et al.*, 2012]. Tropical cyclones, as powerful vortex disturbances in tropical regions, can cause strong perturbations in the ionosphere [Rozhnoi *et al.*, 2014]. For instance, in quiet geophysical conditions an increase in the total electron content (TEC) disturbance intensity over the periods of ranges (02–20 min and 20–60 min) can be observed over tropical cyclones [Polyakova and Perevalova, 2011]. Ionospheric responses to tropical cyclones have been studied using observations from a variety of techniques, such as high frequent (HF) Doppler shift, incoherent scatter radar (ISR), ionosonde, and GPS [e.g., Bishop *et al.*, 2006; Rice *et al.*, 2012; Xiao *et al.*, 2007].

In the 1950s, Bauer [1958] made the first study of a possible ionospheric response following a nearby passage hurricane and found an increase in  $f_oF_2$  with the approach of the storm by analyzing ionosonde data. Afterward, several studies presented the ionospheric responses to tropical cyclones. More recently, Bishop *et al.* [2006] analyzed the ionospheric response to a nearby tropical storm above the Arecibo Observatory using a suite of instruments including ISR, ionosonde, and a satellite-borne GPS receiver. In that analysis,

the ISR observed surprising variations in the  $F$  region plasma drift and the ionosonde observed intense mid-latitude spread  $F$  on the night following the closest passage of the storm. Moreover, GPS occultation within the storm path showed  $F$  region scintillation. From comparisons between 24 strong typhoons recorded from 1987 to 1992 and corresponding ionospheric HF Doppler shift data, Xiao *et al.* [2007] revealed that medium-scale traveling ionospheric disturbances in the ionosphere almost always appear during typhoon events. Rice *et al.* [2012] presented an anomalous 3 day  $f_oF_2$  enhancement in ionosonde observations when a typhoon was passing by Japan and verified this enhanced  $f_oF_2$  anomaly using independent GPS TEC observations. Xiao *et al.* [2012] analyzed two cases of ionospheric daytime spread  $F$  in the period of typhoons using HF Doppler records. Their analysis provided good observational evidence for daytime spread  $F$  during typhoon period in Asian region. A statistical analysis of ionospheric responses to several tropical cyclones based on GPS signals and meteorological data indicate that ionospheric plasma irregularities can occur over cyclone trajectory and that TEC variation intensity is higher if several cyclones simultaneously act in a region [Polyakova and Perevalova, 2011, 2013].

The physical mechanisms responsible for tropical cyclone-ionosphere interaction have also been discussed. A mechanism based on tropical cyclone-generated gravity waves (GWs) has been proposed [Bishop *et al.*, 2006; Polyakova and Perevalova, 2011; Rice *et al.*, 2012; Xiao *et al.*, 2007]. Tropical cyclones are the possible sources of GWs at the ionospheric heights, and they can trigger GWs in the upper troposphere and lower stratosphere (UT/LS) [Chane Ming *et al.*, 2010; Dhaka *et al.*, 2003; Ibrahim *et al.*, 2010; Pfister *et al.*, 1993]. The GWs play an important role in the transport of energy and momentum in the Earth's atmosphere [Hocke and Schlegel, 1996]. It can influence the dynamics as well as distributions of chemical constituents of the Earth's middle atmosphere [Fritts and Alexander, 2003]. When propagating up to ionospheric heights, GWs can induce perturbations of electron density, ion velocity, and ion and electron temperature in the ionosphere [Hocke and Tsuda, 2001; Hooke, 1970; Laštovička, 2006; Millward *et al.*, 1993]. An alternative mechanism is based on the electric field induced by tropical cyclones. The tropical cyclone-ionosphere interactions caused by this mechanism have been discussed in some studies [e.g., Pulinet *et al.*, 2000; Sorokin *et al.*, 2006]. The electric field resulted from the electric charges at the top of a tropical cyclone can penetrate into the ionosphere and cause the increase of electron concentration in the  $F$  layer maximum over the tropical cyclone center [Rozhnoi *et al.*, 2014, and references therein].

In the past, tropical cyclone-ionosphere interaction was studied mainly by examining the variations of ionospheric parameters (e.g.,  $f_oF_2$  and TEC). However, studies on ionospheric irregularities and scintillations associated with tropical cyclones are still very limited. In Hong Kong, a dense network of GNSS Continuously Operating Reference Stations (CORS) has been deployed for precise surveying and mapping, meteorological water vapor monitoring, and other applications. The Hong Kong Satellite Positioning Reference Station Network (SatRef), starting to operate since 2000, consists of 12 GNSS CORS stations. On average, Hong Kong experiences three to four tropical cyclones each year. In addition, two GNSS-based ionosphere scintillation monitoring stations have been in continuous operation in 2012 [Liu *et al.*, 2013]. This paper studies the ionospheric responses to a tropical cyclone via analyzing ionospheric irregularities and the associated scintillations of GPS signals, based on the ionosphere scintillation data collected from one ground-based station in Hong Kong and space-based GPS receivers on board the Constellation Observing System for Meteorology, Ionosphere, and Climate (COSMIC) satellites. This tropical cyclone event occurred during 18–30 August 2012 and passed the Hong Kong region with the closest distance 290 km from Hong Kong at around 17 universal time (UT) on 25 August 2012. Studies of ionospheric perturbations associated with the tropical cyclones can further our understanding of dominant processes and interactions between the ionosphere and the lower atmosphere.

In the following sections, we first described the data set and method used to study a tropical typhoon. Then, the ionospheric irregularities and associated scintillations in GPS signals during the tropical typhoon passage are presented, followed by a discussion of ionospheric responses with the meteorological processes in the lower atmosphere. Finally, a conclusion is given at the end of this paper.

## 2. Data and Method

In the period of 20 to 29 August 2012, the tropical cyclone Tembin took place over the western North Pacific. The trajectory of Tembin is depicted in Figure 1. The red dots represent the location of Tembin at 00:00 UT

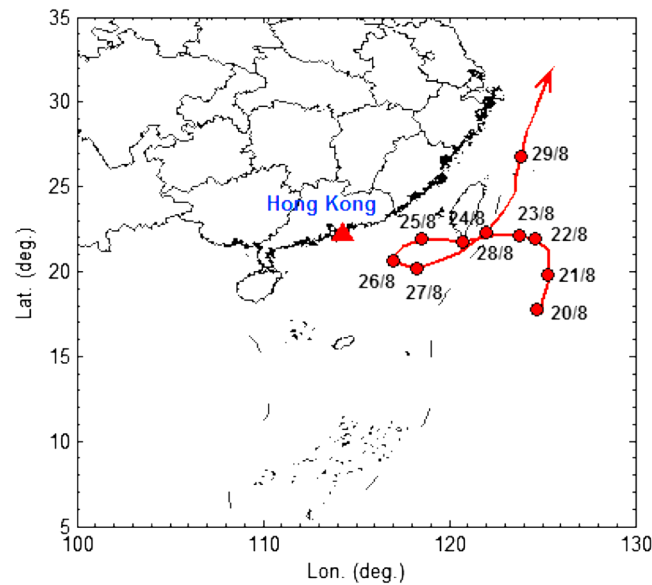


**Figure 1.** Trajectory of tropical cyclone Tembin from 20 August to 29 August 2012. The red dots depict the locations of Tembin at 00:00 UT each day. The red triangle represents the location of scintillation monitoring station at Hok Tsui, Hong Kong.

on each day, and the red triangle indicates the location of the ground-based GNSS-based scintillation monitoring station installed at Hok Tsui, Hong Kong.

As shown in Figure 1, Tembin moved quite erratically during its passage. According to the Tropical Cyclone Annual Publication of the Hong Kong Observatory [Hong Kong Observatory, 2014], the track of Tembin was the most complicated one in 2012. Formed as a tropical depression over the western North Pacific on 18 August 2012, Tembin intensified into a severe typhoon on 20 August, weakened into a typhoon on 22 August, but intensified again into a severe typhoon on 23 August. Entering the northern part of the South China Sea on 24 August, it weakened into a typhoon and had a loop path in the following 2 days. Under the influence of another tropical cyclone Bolaven, Tembin turned to move east-northeastward on 27 August. It weakened into a severe tropical storm on 28 August and a tropical storm on 29 August. Afterward, it became an extratropical cyclone. At around 17 UT on 25 August 2012, Tembin had the closest distance to Hong Kong (about 290 km). After that it moved away in the east-southeast direction.

During the periods when Tembin was passing Hong Kong (within a distance of 800 km), no presence of strong geomagnetic activity or solar activity was observed. The solar  $F_{10.7}$  index, geomagnetic  $K_p$  index, and  $Dst$  index during the Tembin passage period are depicted in Figure 2. As shown in Figure 2, the  $K_p$  values mainly varied between 0 and 4— and the  $Dst$  was quite stable and varied between  $-29$  nT and  $9$  nT. The variation of  $F_{10.7}$  also indicated gentle solar activities when Tembin were passing Hong Kong.

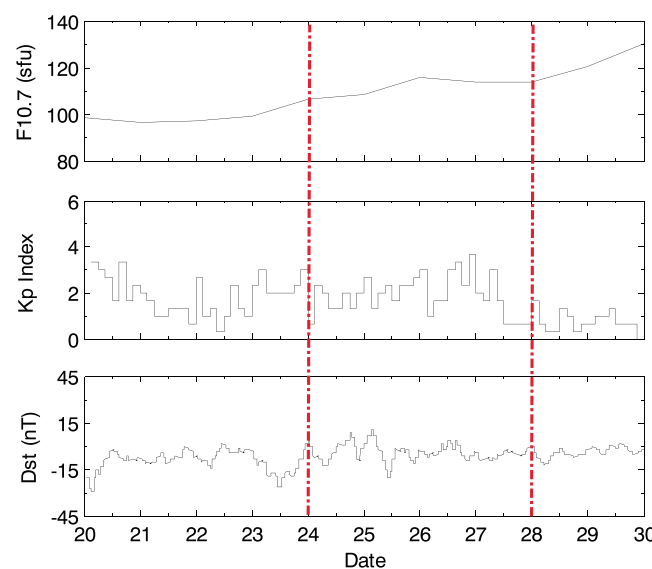


**Figure 2.**  $F_{10.7}$ ,  $K_p$ , and  $Dst$  indices in the period from 20 to 29 August 2012. The periods between the red lines indicate the time when Tembin was passing Hong Kong within a distance of 800 km.

In order to investigate the ionospheric responses to the tropical cyclone Tembin, data collected from a GNSS-based ionospheric scintillation monitoring receiver are analyzed. This GNSS receiver, installed in May 2012 at the Hok Tsui station (geographic:  $22^{\circ}12'N$ ,  $114^{\circ}15'E$ ; geomagnetic:  $12^{\circ}23'N$ ,  $173^{\circ}34'W$ ) of Hong Kong and shown as red triangle in Figure 1, is capable of recording GPS, Global Navigation Satellite System (GLONASS), and Galileo in-phase and quadra-phase data at 100 Hz, and carrier phase measurements at 50 Hz [Liu et al., 2013]. In this study, only GPS data observed above  $15^{\circ}$  elevation angle are considered, in order to reduce the effects of nonscintillation-related tracking errors such as multipath.

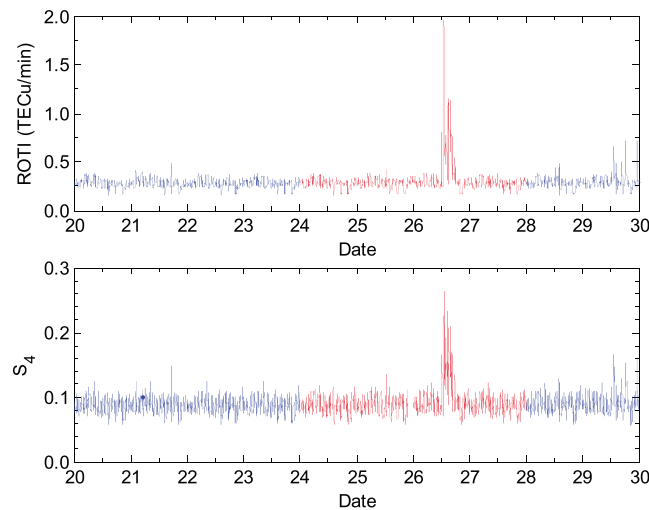


**Figure 3.** The variation of 1 min (top) ROTI and (bottom)  $S_4$  for all satellites during the period of 20 August to 29 August 2012. The ROTI and  $S_4$  during the passage of Tembin with a distance of 800 km from Hong Kong are presented in red.

because the duration of a GPSRO event is usually short and COSMIC satellites have a high speed of movement in the space. For both ground-based and space-based ROTI, the used GPS carrier phase data have 1 Hz sampling rate.

$$ROTI = \sqrt{\langle ROT^2 \rangle - \langle ROT \rangle^2}$$

The amplitude scintillation index  $S_4$  is used to quantify the intensity of scintillations.  $S_4$  is calculated as the standard deviation of the GPS signal intensity (SI) amplitude normalized by its mean value over 60 s for the ground-based observations [Van Dierendonck et al., 1993], and over 1 s for the COSMIC observations [Syndergaard, 2006]. For both ground-based and space-based  $S_4$ , the data's sampling rate is 50 Hz.

$$S_4 = \sqrt{\frac{\langle SI^2 \rangle - \langle SI \rangle^2}{\langle SI \rangle^2}}$$

### 3. Analysis and Results

#### 3.1. Ionospheric Irregularities and Scintillations of Ground-Based GPS Signals

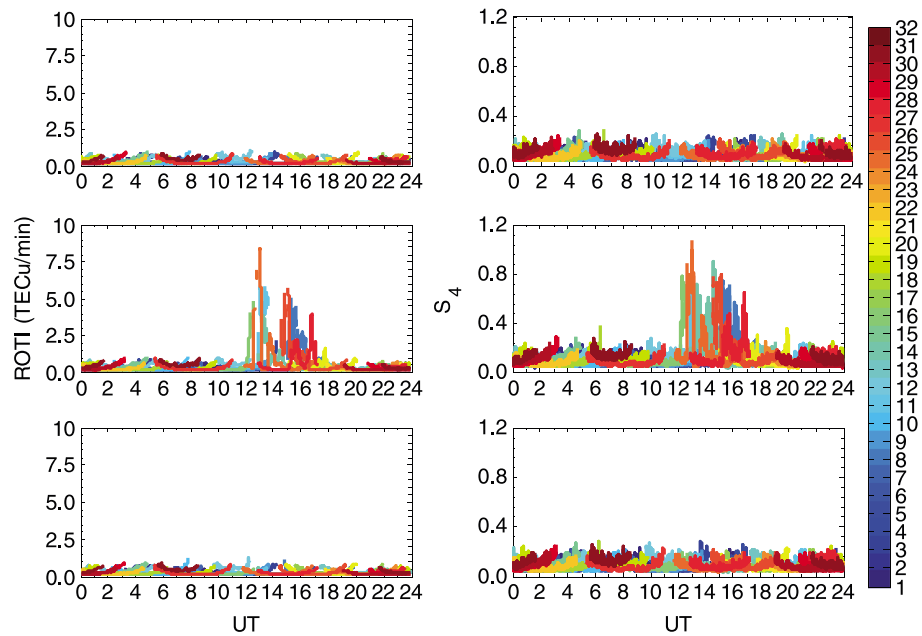
The ionospheric responses to the Tembin tropical cyclone were characterized by the ROTI and amplitude scintillation index  $S_4$ , both of which are derived from GPS data collected at the Hok Tsui station (geographic: 22°12'N, 114°15'E) at Hong Kong. Figure 3 illustrates the variation of 1 min ROTI and  $S_4$  average for all satellites over the period of 20–29 August 2012. The portion in red indicates the results when Tembin was within a distance of 800 km from Hong Kong.

Figure 3 shows that a significant increase in both ROTI and  $S_4$  can be observed on 26 August 2012, while no enhancement was observed on other days. The ROTI generally is at the level of 0.25 TECU/min (1 TECU refers to  $10^{16}$  el  $m^{-2}$ ) and is very stable over the days except 26 August 2012.  $S_4$  generally varies at the level of 0.1 except the day of 26 August. On 26 August, the maximum ROTI reaches nearly 2.0 TECU/min and the maximum  $S_4$  is larger than 0.26. Normally,  $ROTI > 0.5$  TECU/min indicates the presence of ionospheric irregularities at scale lengths of a few kilometers [Ma and Maruyama, 2006].  $S_4 > 0.2$  always indicates nonignorable scintillation activity [Muella et al., 2008]. It is noteworthy that on 26 August Tembin had the closest distance from Hong Kong, as shown in Figure 1.

Figure 4 depicts the temporal variations of ROTI and  $S_4$  observed on 26 August 2012 in a more detailed manner. For comparison purpose, the results on 25 August and 27 August 2012 are also presented. Each GPS

In addition to the ground-based ionospheric scintillation data, the GPS radio occultation (GPSRO) data from the Constellation Observing System for Meteorology, Ionosphere, and Climate (COSMIC) satellites are also used, to study the ionospheric irregularities and scintillations of GPS signals associated with the passage of Tembin. These GPSRO data include 1 s raw GPS data and 1 s scintillation data provided by the COSMIC Data Analysis and Archived Centre (CDAAC).

The rate of change of TEC index (ROTI) defined as the standard deviation of rate of change of TEC (ROT) is used to indicate the presence of ionospheric irregularities [Pi et al., 1997]. For the ground-based observations, the ROTI is calculated over a 5 min period. Space-based ROTI is obtained over a 5 s period



**Figure 4.** The variation of ROTI and  $S_4$  on (top row) 25 August, (middle row) 26 August, and (bottom row) 27 August 2012 over the Hok Tsui station, Hong Kong. Each GPS satellite uses one color to represent its ROTI and  $S_4$  values, as indicated in the color bar.

satellite uses one color to represent its ROTI and  $S_4$  values, as indicated in the color bar. It shows that both ROTI and  $S_4$  have an evident increase on 26 August. The increase began from 12:00 UT (local time = UT + 8 h) and ended before 18:00 UT. It should be noted that the enhancements of ROTI and  $S_4$  agree well in time. As a close view of the ionospheric responses to Tembin, Figure 5 displays the temporal variations of ROTI and  $S_4$  corresponding to the affected GPS satellites (pseudo random noise (PRN) sequences are 9, 15, 17, 26, and 27) in the nighttime period of 26 August 2012. It can be seen from Figure 5 that after sunset starting from 12:00 UT to 18:00 UT these satellites have observed large values of ROTI and  $S_4$ , especially for PRN 26.

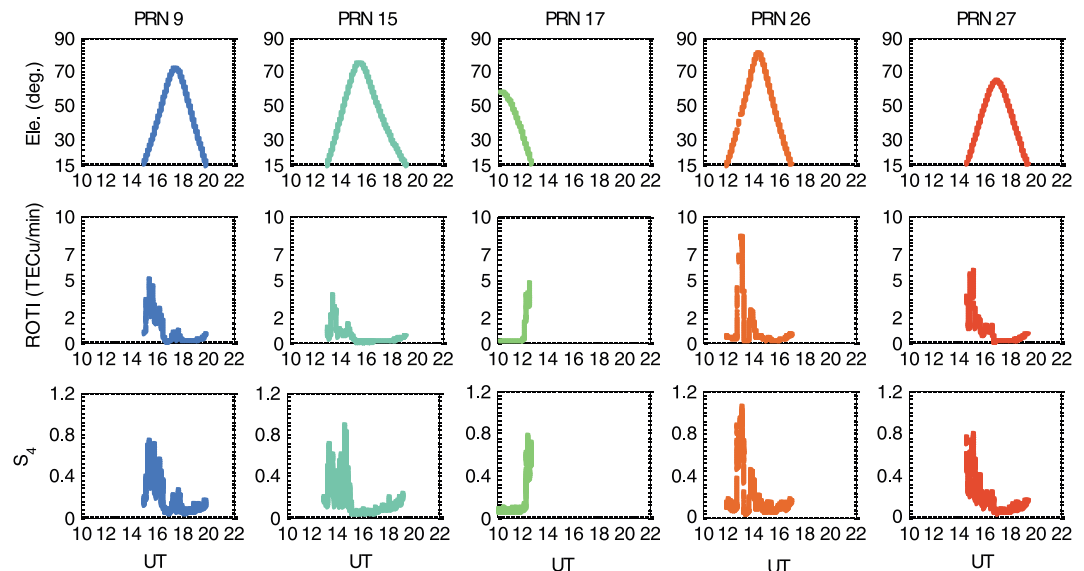


**Figure 5.** The variation of satellite elevation, ROTI, and  $S_4$  for GPS satellites (PRNs 9, 15, 17, 26, and 27) that experience ionospheric irregularities and scintillations on 26 August 2012.

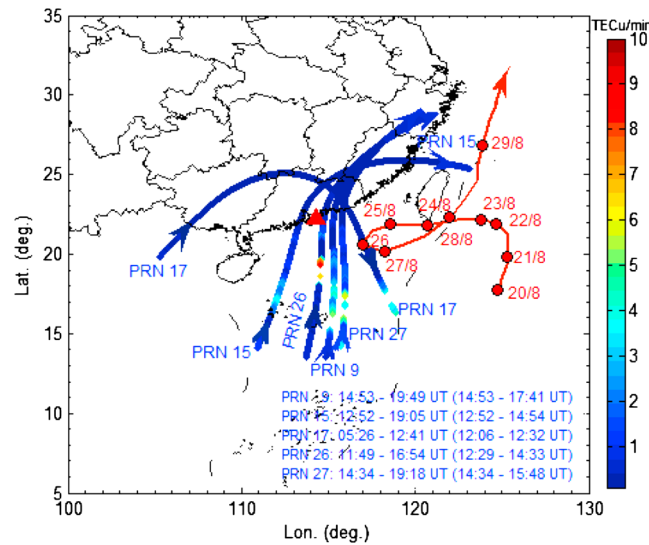


**Figure 6.** The ROTI along the trajectories of GPS satellites (PRNs 9, 15, 17, 26, and 27) that experience ionospheric irregularities and scintillations on 26 August 2012 and the trajectory of the tropical cyclone Tembin (in red). The red triangle represents the Hok Tsui station in Hong Kong. The time period for each satellite tracked by the Hok Tsui station is shown at the right bottom corner and the time period in the parentheses indicates when ROTI > 0.5 TECU/min. The ionospheric pierce points are mapped to the ionospheric layer defined at the altitude of 350 km.

around its path. Specifically, PRNs 9, 15, 26, and 27 satellites experienced large ROTI and  $S_4$  in the period of 12:00–18:00 UT when rising from the south of Hok Tsui station. When descending in the north, they did not show any increase of ROTI or  $S_4$ . Among these affected satellites, PRN 26 satellite had the largest ROTI and  $S_4$  observations. As for the PRN 17 satellite, when its pierce points were very close to the Tembin’s path (before 12:00 UT), there was no evidence of ionospheric irregularities and associated scintillations. When it descended after 12:00 UT, it traveled into the region where other satellites experienced large values of ROTI and  $S_4$ , and it also had a significant increase of ROTI and  $S_4$ . We can see that the trajectories of these satellites, where irregularities and scintillations were observed, were very close to the path of Tembin on 26 August, indicating the possible ionospheric responses to the tropical cyclone Tembin approaching Hong Kong.

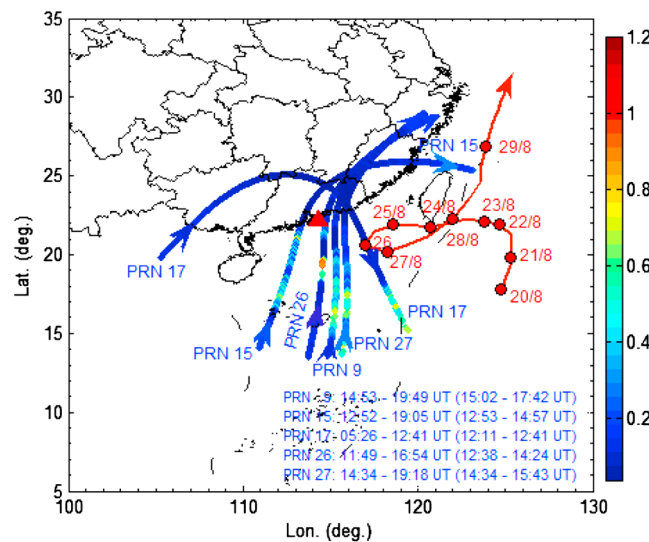


**Figure 7.** The  $S_4$  along the trajectories of GPS satellites (PRNs 9, 15, 17, 26, and 27) that experience ionospheric irregularities and scintillations on 26 August 2012 and the trajectory of the tropical cyclone Tembin (in red). The red triangle represents the Hok Tsui station in Hong Kong. The time period for each satellite tracked by the Hok Tsui station is shown at the right bottom corner and the time period in the parentheses indicates when  $S_4$  > 0.2. The ionospheric pierce points are mapped to the ionospheric layer defined at the altitude of 350 km.

In addition to the temporal variations, the spatial distributions of corresponding ROTI and  $S_4$  for each affected satellite are illustrated in Figures 6 and 7, respectively. In the two figures the trajectories of the satellites are represented by the ionospheric pierce points that are mapped onto the ionospheric layer defined at the altitude of 350 km. The time periods of the affected satellites as well as the trajectory of Tembin are also shown. Referring to Figures 6 and 7 and the satellite elevation change in Figure 5, it is noted that PRNs 9, 15, 26, and 27 satellites rise from the south to the north, and PRN 17 satellite passes from the west to southeast of Hok Tsui station. It should also be noted that PRN 17 did not show significant scintillations when the satellite and Tembin trajectories had the closest distance.

As shown in Figures 6 and 7, the large ROTI and  $S_4$  values observed along the pierce points of these satellites are not rightly over the path of Tembin but around its path. Specifically, PRNs 9, 15, 26, and 27 satellites experienced large ROTI and  $S_4$  in the period of 12:00–18:00 UT when rising from the south of Hok Tsui station. When descending in the north, they did not show any increase of ROTI or  $S_4$ . Among these affected satellites, PRN 26 satellite had the largest ROTI and  $S_4$  observations. As for the PRN 17 satellite, when its pierce points were very close to the Tembin’s path (before 12:00 UT), there was no evidence of ionospheric irregularities and associated scintillations. When it descended after 12:00 UT, it traveled into the region where other satellites experienced large values of ROTI and  $S_4$ , and it also had a significant increase of ROTI and  $S_4$ . We can see that the trajectories of these satellites, where irregularities and scintillations were observed, were very close to the path of Tembin on 26 August, indicating the possible ionospheric responses to the tropical cyclone Tembin approaching Hong Kong.

### 3.2. Ionospheric Irregularities and Scintillations of Spaceborne GPS Signals

The spaceborne GPS observations collected by the GPS receivers on board COSMIC satellites in the period of 20–29 August 2012 are analyzed to further

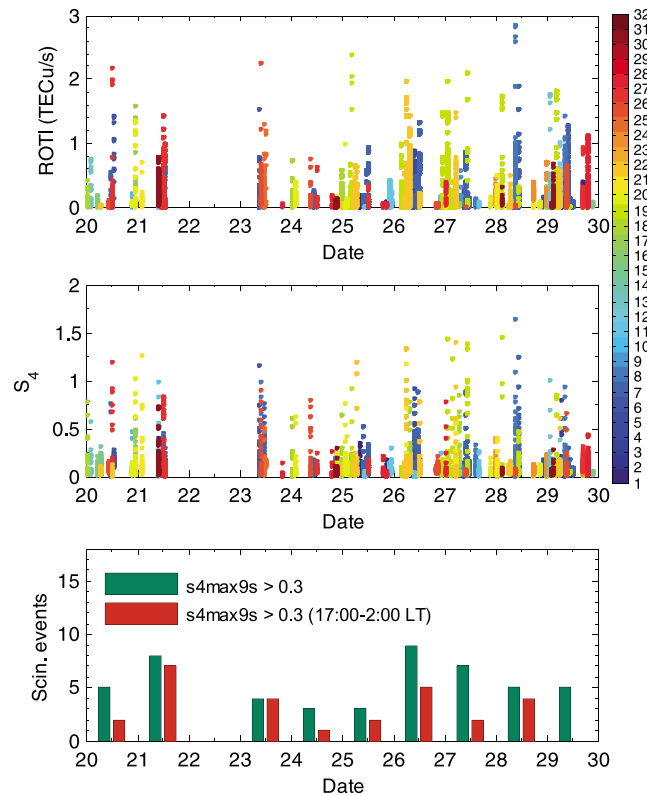


**Figure 8.** The variation of (top) ROTI and (middle)  $S_4$  derived from COSMIC observations in the area within the latitude range of  $12^\circ\text{N} \sim 27^\circ\text{N}$  and longitude range of  $110^\circ\text{E} \sim 130^\circ\text{E}$ , as well as the number of radio occultation scintillation events with (bottom)  $S_4\text{max}9\text{s} > 0.3$  during the period of 20 to 29 August 2012. Each GPS satellite uses one color to represent its ROTI (top) and  $S_4$  (middle) values.

however, it is found that the number of scintillation events with  $S_4\text{max}9\text{s} > 0.3$  peaks on 26 August 2012. Moreover, during the passage of Tembin within a distance of 800 km from Hong Kong (24–27 August), most nighttime scintillation events were observed in the period of 17:00–2:00 LT on 26 August. The results also suggest the ionospheric irregularities and associated scintillations were also dominant on 26 August, as revealed from the ground-based GPS observations.

Compared with the ground-based results shown in Figure 3, the large values of  $S_4$  and ROTI derived from COSMIC data are shown not only on 26 August 2012 but also on other days. This difference may be caused by two reasons. One is different time interval used for the  $S_4$  calculation. The COSMIC  $S_4$  is derived from 1 s using 50 Hz measurements, while the ground-based  $S_4$  is derived from 60 s using 50 Hz data. Another is the different paths of line of sight of GPS signals through the ionosphere. For the COSMIC observations, their path lengths are essentially horizontal. The  $S_4$  index is proportional to the path length through the scintillating medium [Dymond, 2012]. So compared with the ground-based observations, the GPSRO technique is more sensitive to the scintillations as the line of sight has a significant portion in the ionosphere.

With respect to the analysis from the ground-based observations given in Figure 4, the GPSRO scintillation data during nighttime on 25, 26, and 27 August 2012 are examined to show the information on ionospheric irregularities and scintillation in details. Table 1 shows the scintillation information derived from GPS data for each radio occultation event occurring during 9:00–18:00 UT (LT = UT + 8 h) on 25, 26, and 27 August 2012 over the area of  $12^\circ\text{N} \sim 27^\circ\text{N}$  in latitude and  $110^\circ\text{E} \sim 130^\circ\text{E}$  in longitude. In Table 1, the occurrence time, the latitude, longitude, and altitude of the tangent point (point of closest approach to the center of the Earth in the GPSRO path) are all corresponding to the moment when scintillation has the maximum  $S_4$ . The maximum ROTI is also derived and shown in the last column.

study the ionospheric responses to Tembin. In view of the coverage of Tembin's path and the ground-based GPS observations, COSMIC radio occultation events observed in the area of  $12^\circ\text{N} \sim 27^\circ\text{N}$  in latitude and  $110^\circ\text{E} \sim 130^\circ\text{E}$  in longitude are studied. The 10 day time series of ROTI and  $S_4$  derived from all COSMIC satellites over the considered area are illustrated in Figure 8. In addition, the number of daily radio occultation scintillation events defined as  $S_4\text{max}9\text{s}$  (the average  $S_4$  over 9 s around the maximum  $S_4$ )  $> 0.3$  is also presented in the figure. The  $S_4\text{max}9\text{s}$  is preferred to  $S_4\text{max}$  to avoid the outlier of the maximum  $S_4$  [Ko and Yeh, 2010]. It should be mentioned that no COSMIC scintillation data are available over the studied area on 22 August 2012, so no result is shown for that day.

During the 10 day period, the values of  $S_4$  (most within the range of 0~1.5) show a similar variation trend with those of ROTI (most in the range of 0~3 TECU/s), as displayed in Figure 8. It shows that neither  $S_4$  nor ROTI values derived from COSMIC GPS observations show a distinct difference during the passage of Tembin. After a further inspection of scintillation statistics,

**Table 1.** The Scintillation Information Derived From COSMIC Radio Occultation Observations in the Period of 9:00–18:00 UT on 25, 26, and 27 August 2012 Over the Area of 12°N ~ 27°N in Latitude and 110°E ~ 130°E in Longitude

Date	Time (UT)	GPS PRN	COSMIC Satellite ID	Latitude (deg)	Longitude (deg)	Tangent Alt. (km)	S <sub>4</sub> max	ROTI <sub>max</sub> (TECU/s)
25 August	09:56:53	8	2	19.98	111.39	109.578	0.534	1.462
	11:44:13	8	5	20.01	123.77	98.530	0.344	0.938
26 August	09:38:32	5	5	26.44	117.64	107.850	0.928	0.892
	09:50:38	8	1	20.89	119.17	106.490	0.748	0.478
	11:17:24	8	5	18.15	124.92	57.238	0.475	0.513
	11:35:22	8	1	15.64	119.05	105.217	0.890	0.547
27 August	11:46:57	23	1	15.33	125.96	105.061	0.785	0.754
	09:21:42	8	1	26.34	115.41	115.326	0.888	0.868
	10:50:03	8	5	16.48	123.92	94.823	0.365	0.209

Compared with the results for the other 2 days, more scintillations with large values of S<sub>4</sub>max were recorded by the COSMIC GPSRO observations during the period of 9:00–18:00 UT on 26 August 2012, as shown in Table 1. On this day the occulted GPS satellites included PRNs 5, 8, and 23, and the RO scintillations were predominantly observed near the sunset time when ionospheric irregularities and scintillations were also observed by the ground-based GNSS receiver. The maximum S<sub>4</sub> and ROTI observed on 26 August were in the ranges of 0.475 ~ 0.928 and 0.478 ~ 0.892 TECU/s, respectively, and they were mainly observed at the tangent altitudes of 57.238 ~ 107.850 km. For the other 2 days, only GPS satellite PRN 8 was occulted with large

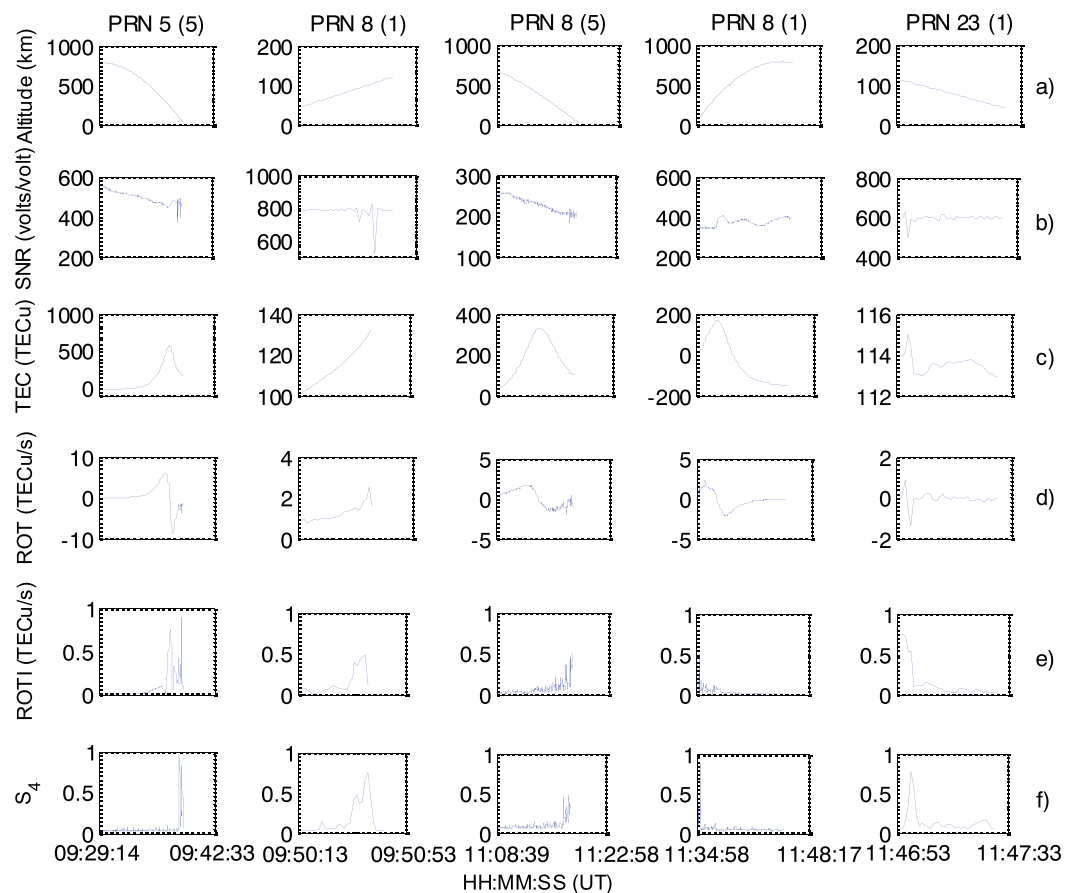


**Figure 9.** (a) The altitudinal information for the tangent points of each RO scintillation. The temporal variations of (b) L1 C/A code signal-to-noise ratio (SNR), (c) uncalibrated TEC, (d) ROT, (e) ROTI, and (f) S<sub>4</sub> are derived from COSMIC observations for GPS satellites (PRNs 5, 8, and 23) that experience ionospheric irregularities and scintillations on 26 August 2012. The COSMIC satellite number is given in the parenthesis after the PRN of GPS satellite.

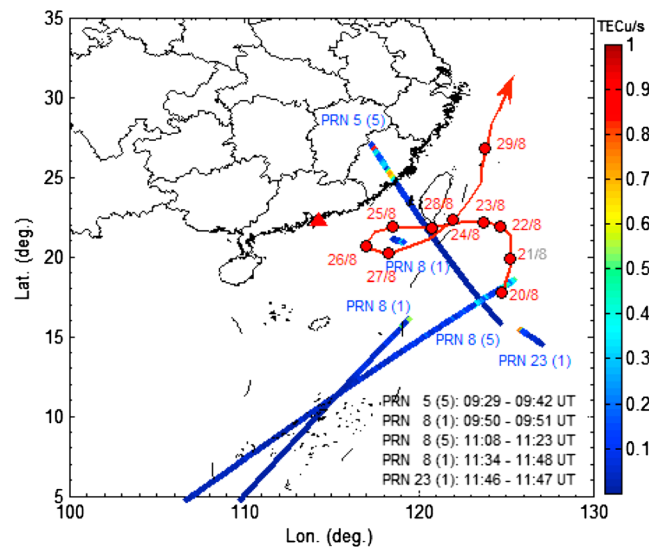


**Figure 10.** The ROTI along the tangent points of the COSMIC radio occultation events for GPS satellites (PRNs 5, 8, and 23) that experienced ionospheric irregularities and scintillations on 26 August 2012 and the trajectory of Tembin (in red). The red triangle represents the Hok Tsui GPS scintillation monitoring station in Hong Kong. The time period for each occulted satellite is shown at the right corner. The COSMIC satellite number is given in the parenthesis behind the GPS PRN number.

S4max. The large number of affected GPS satellites on 26 August 2012 indicates that ionosphere irregularity has been very likely created when the Tembin passed Hong Kong.

It should be noted from Table 1 and Figure 8 that the magnitude of ROTI derived from the COSMIC observations is much larger than that from the ground-based observations. For instance, in Table 1 the maximum ROTI on 26 August 2012 reaches 0.892 TECU/s, which is equivalent to 53.5 TECU/min, while the ROTI derived from ground-based observations is less than 10 TECU/min (see Figure 5). The large magnitude of ROTI from the COSMIC observations may be related to two factors. One is the high-speed movement of the GPS receiver on board COSMIC satellites. The length of GPS signal passing through the ionosphere varies rapidly. The magnitude of ROTI can be larger for satellites with higher velocities and for higher iono-

spheric drifts [Basu et al., 1999]. One is that the ROTI for using the COSMIC data was calculated over a 5 s period, while the ground-based ROTI was estimated over a 5 min period. The length of scintillation observation time is much short due to the high speed of space-based GPS receiver; thus, a shorter period is used. Though the ROTI derived from COSMIC observations has a larger magnitude, it is still able to characterize the ionospheric irregularities, as can be seen from its consistent variation with S4 shown in Figure 8.

The detailed information on the temporal variations of the L1 C/A code signal-to-noise ratio (SNR), uncalibrated TEC, ROT, ROTI, and S4 derived from the COSMIC GPSRO observations corresponding to the affected GPS satellites (PRNs 5, 8, and 23) on 26 August 2012 is illustrated in Figure 9. In addition, the altitudinal information for the tangent points of each RO path is also given in Figure 9a to illustrate the variation of TEC, ROT, ROTI, and S4 with respect to tangent altitude. As illustrated in Figure 9, rapid TEC fluctuations can be observed with the increase of ROTI and S4, and the ROTI and S4 show a consistent increase with the decrease of SNR. The remarkable increases suggest that ionospheric irregularities and associated scintillations occurred in the GPSRO observations. For each GPSRO observation, the scintillation region along the line of sight can be geolocated to its tangent point [Dymond, 2012; Ko and Yeh, 2010]. So the altitude of the tangent points indicates the ionospheric irregularities and scintillations of GPS RO signals may be observed at the altitude range of 60 ~ 120 km, which can also be seen from Table 1. The results presented in Table 1 and Figures 8 and 9 suggest that on 26 August the ionospheric responses to Tembin may be observed by the GPS receivers on board the COSMIC satellites.

Apart from the temporal variation shown in Figure 9, the spatial distributions of ROTI and S4 along the tangent points of RO observations of GPS satellites (PRNs 5, 8, and 23) that experienced ionospheric irregularities and scintillations on 26 August 2012 were displayed in Figures 10 and 11, respectively. As shown in the figures, the ROTI and S4 increased consistently and their maximum took place near the path of Tembin. Note that the PRN 8 and 23 satellites experienced large values of ROTI and S4 dominantly in the southeast of Hong Kong, while the PRN 5 had large results in the northeast area. It appears that the locations of the PRN 8 (Lat: 15.64°N, Lon: 119.05°E) at 11:35 UT are very close to the trajectory of PRN 17 satellite tracked by the ground-based GNSS receiver at around 12:00 UT. It is worthwhile mentioning that ionospheric irregularities and scintillations were seen in the GPS signals for these two satellites, as also shown in Figures 5 and 9. This shows that ionospheric responses to Tembin were concurrently observed by both ground-based and space-based GNSS receivers on 26 August 2012.

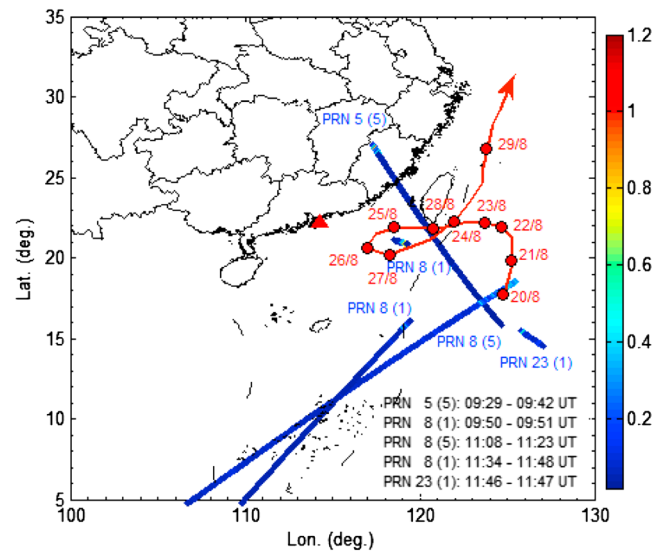


**Figure 11.** The  $S_4$  along the tangent points of the COSMIC radio occultation events for GPS satellites (PRNs 5, 8, and 23) that experienced ionospheric irregularities and scintillations on 26 August 2012 and the trajectory of Tembin (in red). The red triangle represents the Hok Tsui GPS scintillation monitoring station in Hong Kong. The time period for each occulted satellite is shown at the right corner. The COSMIC satellite number is given in the parenthesis behind the GPS PRN number.

In the analysis and comparison of space-based and ground-based scintillation data, a few factors need to be considered. Compared with ground-based observations illustrated in Figures 6 and 7, the region where the COSMIC observations have large values of ROTI and  $S_4$  extends more widely. The ray path geometry of COSMIC observations is different from that of ground-based observations, and only limited COSMIC observations are available over the studied region. In COSMIC observation study the tangent point is used to represent the spatial location of ionospheric irregularities and scintillations, while the ionospheric pierce point is used for ground-based observations. In addition, the uncertainty of tangent points should also be considered, as the location of the tangent point sometimes can have an error of  $\sim 10^\circ$  [Dymond, 2012].

#### 4. Discussion

In the absence of strong geomagnetic and solar activities, nighttime ionospheric irregularities and scintillations of GPS signals were observed in both ground-based and spaceborne observations when Tembin passed closely to Hong Kong on 26 August 2012. Their spatial occurrences (see Figures 6, 7, 10, and 11) indicate that they are mainly observed in the south of Hong Kong within the latitude range of  $13^\circ\text{N} \sim 23^\circ\text{N}$  and longitude range of  $110^\circ\text{E} \sim 120^\circ\text{E}$ . This should be ascribed to the location of the station in the equatorial ionospheric anomaly region [Abadi *et al.*, 2014].

The mechanism responsible for equatorial ionospheric irregularities and scintillations has been widely discussed. It is generally accepted that the Rayleigh-Taylor instability process in the bottom side of the  $F$  region is the mechanism to explain the generation of ionospheric plasma bubbles and associated scintillations [Aarons, 1982; Dandekar and Groves, 2004]. After sunset, a rapidly increased eastward electric field causes an uplift of the  $F$  layer. The vertical upwelling of the ionosphere leads to steep density gradients in the bottomside  $F$  region and becomes an unstable situation. This situation eventually leads to the formation of plasma bubbles that develop irregularities to produce severe scintillations.

Several works have pointed out gravity waves as a possible seeding mechanism of the ionospheric plasma bubbles [Nicolls and Kelley, 2005; Singh *et al.*, 1997; Taori *et al.*, 2011]. As already mentioned earlier, the tropical cyclones can trigger gravity waves in the upper troposphere and lower stratosphere. According to the studies [Abdu *et al.*, 2009; Fritts *et al.*, 2008; Takahashi *et al.*, 2009, and references therein], the gravity waves generated in the tropospheric convective regions are upward at slant angle through the mesosphere and the thermosphere. When propagating up to the bottomside  $F$  layer in the ionosphere, these waves can induce electron density perturbation and electric field perturbation. Under right conditions of the ambient ionosphere, these perturbations can initiate the growth of the Rayleigh-Taylor instability leading to vertical development of bubbles to topside ionosphere under typical state of the background ionosphere in the sunset period.

It has been discussed that the gravity waves reaching 100–220 km can produce  $F$  region disturbances via perturbing the plasma and producing electric field variations [Bishop *et al.*, 2006]. The electric field perturbations can contribute to the growth of Rayleigh-Taylor instability leading to the irregularities in the  $F$  region base [Prakash, 1999]. In view of this, it is thus suspected that the occurrence of ionospheric irregularities and

scintillations of GPS signals during the passage of Tembin might be caused by the presence of tropical cyclone-generated gravity waves. The gravity waves generated in the tropospheric convective regions slantly propagate up to the ionospheric height [Abdu *et al.*, 2009], so the spatial distribution of the ionospheric responses observed in the ground- and space-based data is not rightly over the path of Tembin but around its path (see Figures 6, 7, 10, and 11).

It is noteworthy that during the passage of Tembin the ionospheric irregularities and associated scintillations were predominantly recorded on 26 August 2012. One of reasons might be related to the conditions for gravity waves seeding the plasma density instability. If contributing to the instability, the gravity wave should penetrate into the *F* layer bottom height and initiate the instability during the period of *F* layer uplifting. Additionally, the gravity wave should have sufficient amplitude of oscillation and phase speeds to trigger the instability and get a resonance condition for coupling of a wave and plasma process [Takahashi *et al.*, 2009]. In addition to the seed perturbations in the form of gravity waves arising from the tropospheric convective regions, it should be also noted that there are other possible factors affecting day-to-day variability of ionospheric irregularity, including the vertical drift of *F* layer and the meridional wind and field line integrated conductivity [Abdu, 2001]. The varied combinations of background electron density gradient, *F* layer vertical drift velocity, and neutral wind system play a dominant role in the day-to-day variability of irregularities [Hajra *et al.*, 2012]. Another reason might be related to the limited observation coverage of the ground-based GNSS-based scintillation monitoring station and space-based RO. Tembin had a long passage path and some ionospheric responses to Tembin may have not be recorded by either ground-based station or space-based RO. Nevertheless, this observational study still contributes to increasing the knowledge of the interaction between the tropical cyclones and the ionosphere via presenting the ionospheric irregularities and associated scintillations in GPS signals and raising the attention of scintillation effects on the GNSS signals during the passage of tropical cyclones. In addition, the utilization of ROTI derived from the COSMIC observations suggests the feasibility of using spaceborne GPS observations to study ionospheric irregularities even with short period of scintillation data.

## 5. Conclusions

The ionospheric irregularities and associated scintillations of GPS signals occurring during the passage of the Typhoon Tembin approaching Hong Kong are illustrated in this study, utilizing the indices ROTI and amplitude scintillation  $S_4$ . Both indices are derived from the observations collected from a GNSS-based scintillation monitoring station installed in Hong Kong and spaceborne GPS receivers on board COSMIC satellites. Our analysis shows the following.

On 26 August 2012 when the Tembin approached very close to Hong Kong, the ground-based GPS observations revealed the occurrence of ionospheric irregularities and associated scintillations in the nighttime period of 20:00–2:00 LT, and their spatial occurrences in the south of Hong Kong, over the region of 13°N ~ 23°N latitude and 110°E ~ 120°E longitude. From the COSMIC GPSRO observations, it shows that near the sunset period of 18:00–20:00 LT the ionospheric irregularities were observed in the altitude range of 60 ~ 120 km. The analysis also shows that the ionospheric responses to Tembin were concurrently observed by both ground- and space-based observations on 26 August. In the absence of strong geomagnetic and solar activity, it is suspected that gravity waves might have been generated at the lower atmosphere and contributed to the tropical cyclone-ionosphere interaction. They may initiate the growth of Rayleigh-Taylor instability, leading to ionospheric irregularities and associated scintillations of GPS signals.

This study presents possible ionospheric responses to a typhoon from aspects of the ionospheric irregularities and associated scintillations in ground- and space-based GPS signals characterized by the ROTI and  $S_4$  indices. Meanwhile, it also suggests that the passage of tropical cyclones could degrade GNSS signal quality through the ionospheric effects in the tropical cyclone-ionosphere interaction.

## References

- Aarons, J. (1982), Global morphology of ionospheric scintillations, *Proc. IEEE*, 70(4), 360–378.
- Abadi, P., S. Saito, and W. Srigutomo (2014), Low-latitude scintillation occurrences around the equatorial anomaly crest over Indonesia, *Ann. Geophys.*, 32(1), 7–17.
- Abdu, M. (2001), Outstanding problems in the equatorial ionosphere–thermosphere electrodynamics relevant to spread *F*, *J. Atmos. Sol. Terr. Phys.*, 63(9), 869–884.

### Acknowledgments

This work is supported by the Hong Kong Research Grants Council (RGC) Early Career Scheme (ECS) (project PolyU 5325/12E (F-PP0F)) and RGC General Research Fund (GRF) (project PolyU 5203/13E (B-Q37X)). The support from the National Natural Science Foundation of China (NSFC 41274039) is gratefully acknowledged. Zhizhao Liu also thanks the support of the Program of Introducing Talents of Discipline to Universities (Wuhan University, GNSS Research Center), China. The authors would like to thank the COSMIC Data Analysis and Archive Center (CDACC) for providing COSMIC data and the Hong Kong Observatory for providing the information on tropical cyclones in their website at <http://www.hko.gov.hk/publica/pubtch.htm>.

- Abdu, M., E. Alam Kherani, I. Batista, E. de Paula, D. Fritts, and J. Sobral (2009), Gravity wave initiation of equatorial spread *F*/plasma bubble irregularities based on observational data from the SpreadFEx campaign, *Ann. Geophys.*, *27*(7), 2607–2622.
- Basu, S., et al. (1996), Scintillations, plasma drifts, and neutral winds in the equatorial ionosphere after sunset, *J. Geophys. Res.*, *101*, 26,795–26,809, doi:10.1029/96JA00760.
- Basu, S., K. Groves, J. Quinn, and P. Doherty (1999), A comparison of TEC fluctuations and scintillations at Ascension Island, *J. Atmos. Sol. Terr. Phys.*, *61*(16), 1219–1226.
- Bauer, S. J. (1958), An apparent ionospheric response to the passage of hurricanes, *J. Geophys. Res.*, *63*, 265–269, doi:10.1029/JZ063i001p00265.
- Bhattacharyya, A., S. Basu, K. Groves, C. Valladares, and R. Sheehan (2002), Effect of magnetic activity on the dynamics of equatorial *F* region irregularities, *J. Geophys. Res.*, *107*(A12), 1489, doi:10.1029/2002JA009644.
- Bishop, R., N. Aponte, G. Earle, M. Sulzer, M. Larsen, and G. Peng (2006), Arecibo observations of ionospheric perturbations associated with the passage of Tropical Storm Odette, *J. Geophys. Res.*, *111*, A11320, doi:10.1029/2006JA011668.
- Caton, R., and K. Groves (2006), Longitudinal correlation of equatorial ionospheric scintillation, *Radio Sci.*, *41*, RS5522, doi:10.1029/2005RS003357.
- Chane Ming, F., Z. Chen, and F. Roux (2010), Analysis of gravity-waves produced by intense tropical cyclones, *Ann. Geophys.*, *28*(2), 531–547.
- Chernogovskaya, M., B. Shpynev, and K. Ratovsky (2015), Meteorological effects of ionospheric disturbances from vertical radio sounding data, *J. Atmos. Sol. Terr. Phys.*, *136*, 235–243.
- Dandekar, B., and K. Groves (2004), Using ionospheric scintillation observations for studying the morphology of equatorial ionospheric bubbles, *Radio Sci.*, *39*, RS3010, doi:10.1029/2003RS003020.
- Dhaka, S., M. Takahashi, Y. Shibagaki, M. Yamanaka, and S. Fukao (2003), Gravity wave generation in the lower stratosphere due to passage of the typhoon 9426 (Orchid) observed by the MU radar at Shigaraki (34.85 N, 136.10 E), *J. Geophys. Res.*, *108*(D19), 4595, doi:10.1029/2003JD003489.
- Dymond, K. F. (2012), Global observations of L band scintillation at solar minimum made by COSMIC, *Radio Sci.*, *47*, RS0L18, doi:10.1029/2011RS004931.
- Fritts, D., S. Vadas, D. Rigin, M. Abdu, I. Batista, H. Takahashi, A. Medeiros, F. Kamalabadi, H. Liu, and B. G. Fejer (2008), Gravity wave and tidal influences on equatorial spread *F* based on observations during the Spread *F* Experiment (SpreadFEx), *Ann. Geophys.*, *26*(11), 3235.
- Fritts, D. C., and M. J. Alexander (2003), Gravity wave dynamics and effects in the middle atmosphere, *Rev. Geophys.*, *41*(1), 1003, doi:10.1029/2001RG000106.
- Goncharenko, L., and S. R. Zhang (2008), Ionospheric signatures of sudden stratospheric warming: Ion temperature at middle latitude, *Geophys. Res. Lett.*, *35*, L21103, doi:10.1029/2008GL035684.
- Hajra, R., S. Chakraborty, S. Mazumdar, and S. Alex (2012), Evolution of equatorial irregularities under varying electrodynamic conditions: A multitechnique case study from Indian longitude zone, *J. Geophys. Res.*, *117*, A08331, doi:10.1029/2012JA017808.
- Hey, J., S. Parsons, and J. Phillips (1946), Fluctuations in cosmic radiation at radio frequencies, *Nature*, *158*(23), 582.
- Hocke, K., and K. Schlegel (1996), A review of atmospheric gravity waves and travelling ionospheric disturbances: 1982–1995, *Ann. Geophys.*, *14*(9), 917.
- Hocke, K., and T. Tsuda (2001), Gravity waves and ionospheric irregularities over tropical convection zones observed by GPS/MET radio occultation, *Geophys. Res. Lett.*, *28*, 2815–2818, doi:10.1029/2001GL013076.
- Hong Kong Observatory (2014), *Tropical Cyclones in 2012*, edited, Hong Kong Observatory, Hong Kong. [Available at <http://www.hko.gov.hk/publica/tc/TC2012.pdf>]
- Hooke, W. H. (1970), Ionospheric response to internal gravity waves: 3. Changes in the densities of the different ion species, *J. Geophys. Res.*, *75*, 7239–7243, doi:10.1029/JA075i034p07239.
- Ibrahim, C., F. Chane-Ming, C. Barthe, and Y. Kuleshov (2010), Diagnosis of tropical cyclone activity through gravity wave energy density in the southwest Indian Ocean, *Geophys. Res. Lett.*, *37*, L09807, doi:10.1029/2010GL042938.
- Jiao, Y., Y. T. Morton, S. Taylor, and W. Pelgrum (2013), Characterization of high-latitude ionospheric scintillation of GPS signals, *Radio Sci.*, *48*, 698–708, doi:10.1002/2013RS005259.
- Kazimirovsky, E. S. (2002), Coupling from below as a source of ionospheric variability: A review, *Ann. Geophys.*, *45*(1), 1–29.
- Kintner, P. M., B. M. Ledvina, and E. R. de Paula (2007), GPS and ionospheric scintillations, *Space Weather*, *5*, S09003, doi:10.1029/2006SW000260.
- Ko, C., and H. Yeh (2010), COSMIC/FORMOSAT-3 observations of equatorial *F* region irregularities in the SAA longitude sector, *J. Geophys. Res.*, *115*, A11309, doi:10.1029/2010JA015618.
- Korenkov, Y. N., et al. (2012), The global thermospheric and ionospheric response to the 2008 minor sudden stratospheric warming event, *J. Geophys. Res.*, *117*, A10309, doi:10.1029/2012JA018018.
- Laštovička, J. (2006), Forcing of the ionosphere by waves from below, *J. Atmos. Sol. Terr. Phys.*, *68*(3), 479–497.
- Liu, Z. Z., R. Xu, M. Yu, J. S. Xu, W. Pelgrum, S. Taylor, W. Chen, and X. L. Ding (2013), A comparison of GPS-based ionospheric scintillation observations in North and South Hong Kong, paper presented at ION Pacific PNT.
- Ma, G., and T. Maruyama (2006), A super bubble detected by dense GPS network at east Asian longitudes, *Geophys. Res. Lett.*, *33*, L21103, doi:10.1029/2006GL027512.
- Millward, G., R. Moffett, S. Quegan, and T. Fuller-Rowell (1993), Effects of an atmospheric gravity wave on the midlatitude ionospheric *F* layer, *J. Geophys. Res.*, *98*, 19,173–19,179, doi:10.1029/93JA02093.
- Muella, M., E. de Paula, I. Kantor, I. Batista, J. Sobral, M. Abdu, P. Kintner, K. Groves, and P. Smorigo (2008), GPS L-band scintillations and ionospheric irregularity zonal drifts inferred at equatorial and low-latitude regions, *J. Atmos. Sol. Terr. Phys.*, *70*(10), 1261–1272.
- Nicolls, M. J., and M. C. Kelley (2005), Strong evidence for gravity wave seeding of an ionospheric plasma instability, *Geophys. Res. Lett.*, *32*, L05108, doi:10.1029/2004GL020737.
- Pfister, L., K. Chan, T. Bui, S. Bowen, M. Legg, B. Gary, K. Kelly, M. Proffitt, and W. Starr (1993), Gravity waves generated by a tropical cyclone during the STEP tropical field program: A case study, *J. Geophys. Res.*, *98*, 8611–8638, doi:10.1029/92JD01679.
- Pi, X., A. Mannucci, U. Lindqwister, and C. Ho (1997), Monitoring of global ionospheric irregularities using the worldwide GPS network, *Geophys. Res. Lett.*, *24*, 2283–2286, doi:10.1029/97GL02273.
- Polyakova, A., and N. Perevalova (2011), Investigation into impact of tropical cyclones on the ionosphere using GPS sounding and NCEP/NCAR Reanalysis data, *Adv. Space Res.*, *48*(7), 1196–1210.
- Polyakova, A., and N. Perevalova (2013), Comparative analysis of TEC disturbances over tropical cyclone zones in the North–West Pacific Ocean, *Adv. Space Res.*, *52*(8), 1416–1426.

- Prakash, S. (1999), Production of electric field perturbations by gravity wave winds in the E region suitable for initiating equatorial spread F, *J. Geophys. Res.*, *104*, 10,051–10,069, doi:10.1029/1999JA900028.
- Pulinets, S., K. Boyarchuk, V. Hegai, V. Kim, and A. Lomonosov (2000), Quasielectrostatic model of atmosphere-thermosphere-ionosphere coupling, *Adv. Space Res.*, *26*(8), 1209–1218.
- Rice, D., J. Sojka, J. Eccles, and R. Schunk (2012), Typhoon Melor and ionospheric weather in the Asian sector: A case study, *Radio Sci.*, *47*, RS0L05, doi:10.1029/2011RS004917.
- Rozhnoi, A., M. Solovieva, B. Levin, M. Hayakawa, and V. Fedun (2014), Meteorological effects in the lower ionosphere as based on VLF/LF signal observations, *Nat. Hazards Earth Syst. Sci.*, *14*(10), 2671–2679.
- Shi, J., G. Wang, B. Reinisch, S. Shang, X. Wang, G. Zherebotsov, and A. Potekhin (2011), Relationship between strong range spread F and ionospheric scintillations observed in Hainan from 2003 to 2007, *J. Geophys. Res.*, *116*, A08306, doi:10.1029/2011JA016806.
- Singh, S., F. Johnson, and R. Power (1997), Gravity wave seeding of equatorial plasma bubbles, *J. Geophys. Res.*, *102*, 7399–7410, doi:10.1029/96JA03998.
- Sorokin, V., A. Yaschenko, V. Chmyrev, and M. Hayakawa (2006), DC electric field formation in the mid-latitude ionosphere over typhoon and earthquake regions, *Phys. Chem. Earth Parts A/B/C*, *31*(4), 454–461.
- Syndergaard, S. (2006), COSMIC S4 Data. [Available at [http://cdaac-www.cosmic.ucar.edu/cdaac/doc/documents/s4\\_description.pdf](http://cdaac-www.cosmic.ucar.edu/cdaac/doc/documents/s4_description.pdf).]
- Takahashi, H., M. J. Taylor, P. Pautet, A. Medeiros, D. Gobbi, C. Wrasse, J. Fechine, M. Abdu, I. Batista, and E. de Paula (2009), Simultaneous observation of ionospheric plasma bubbles and mesospheric gravity waves during the SpreadFEx Campaign, *Ann. Geophys.*, *27*(4), 1477.
- Taori, A., A. Patra, and L. Joshi (2011), Gravity wave seeding of equatorial plasma bubbles: An investigation with simultaneous F region, E region, and middle atmospheric measurements, *J. Geophys. Res.*, *116*, A05310, doi:10.1029/2010JA016229.
- Van Dierendonck, A., J. Klobuchar, and Q. Hua (1993), Ionospheric scintillation monitoring using commercial single frequency C/A code receivers, paper presented at Proceedings of ION GPS.
- Xiao, S., J. Shi, D. Zhang, Y. Hao, and W. Huang (2012), Observational study of daytime ionospheric irregularities associated with typhoon, *Sci. China: Technol. Sci.*, *55*(5), 1302–1304.
- Xiao, Z., S. Xiao, Y. Hao, and D. Zhang (2007), Morphological features of ionospheric response to typhoon, *J. Geophys. Res.*, *112*, A04304, doi:10.1029/2006JA011671.